Applied Surface Science 257 (2011) 4597–4602

Contents lists available at ScienceDirect

Applied Surface Science

journal homepage: www.elsevier.com/locate/apsusc

Copper nanoparticles grown under hydrogen: Study of the surface oxide

D.E. Diaz-Droguett[a,*], R. Espinoza[b], V.M. Fuenzalida[a]

[a] Departamento de Física, Facultad de Ciencias Físicas y Matemáticas, Universidad de Chile, Santiago, Chile
[b] Departamento de Ciencias de los Materiales, Facultad de Ciencias Físicas y Matemáticas, Universidad de Chile, Santiago, Chile

ARTICLE INFO

Article history:
Received 20 October 2010
Received in revised form
13 December 2010
Accepted 14 December 2010
Available online 21 December 2010

Keywords:
Copper nanoparticles
Hydrogen
Oxide
Surface
Gas condensation

ABSTRACT

Copper nanoparticles with sizes between 10 nm and 50 nm were grown by condensation in hydrogen at pressures from 10 Pa to 1200 Pa. The crystallite size ranged from 10 nm to 25 nm using the Scherrer method. X-ray diffraction showed the reflections of metallic copper occasionally mixed with an oxidized phase (CuO or Cu_2O). As shown by TEM examination, the smaller particles that did not exceed 25 nm exhibited faceted morphologies whereas the bigger ones had ovaled-spherical forms sometimes containing twins. X-ray photoelectron spectroscopy revealed that the nanoparticles consist of a copper core, completely surrounded by a Cu_2O shell, which is oxidized to CuO at the surface layer.

1. Introduction

Copper nanoparticles have attracted attention because of their catalytic [1], optical [2] and electrical properties [3], as well as for their antimicrobial applications [4–6] and industrial uses as additives in lubricants [7] and inks [8]. Nanoparticles possess a large fraction of surface atoms per unit volume that leads to increasing the total surface energy and hence the reactivity with atoms or molecules of the surrounding environment. Copper nanoparticles are highly reactive to air, generating copper oxide on the surface when exposed. The oxide layer formed can be of Cu_2O, CuO or a mixture. Cu_2O and CuO are p-type semiconductors with a direct band gap of about 2.2 eV and 1.2 eV, respectively [9,10], which have been studied as materials for the manufacture of photovoltaic and photoelectrochemical cells [11,12]. Semiconductor oxide nanoparticles are used as a base for gas sensors where the existence of the metallic core, within the oxide shell, can improve the sensor sensitivity and selectivity [13]. The identification of the surface oxidation states of the copper nanoparticles as well as the structural characteristics of the oxide layer and the morphology of the particles are critical to understanding their physical properties and chemical behavior.

Copper nanoparticles have been synthesized through different methods such as the polyol method [14], solvothermal method [15], copper salt reduction [16], electro-reduction in an ionic liquid [17], thermal decomposition [18], laser ablation [19], electron beam irradiation [20] and microwave heating [21]. Another method for fabricating copper nanoparticles is the inert gas condensation (IGC) method. This method consists of a resistive source that evaporates the material at a low pressure (typically ~600 Pa) of a non-reactive carrier gas [22,23]. In this pressure the mean free path in the gas is in the submillimeter range and transport is dominated by collisions, which are diffusive and convective but not ballistic. Therefore, the atoms or molecules of the evaporated material collide with the molecules of the carrier gas, thereby cooling them down. Collisions among the material molecules lead to homogeneous nucleation and growth of nanoparticles, which can be collected onto a cold surface. Empirically, the size of the particles can be diminished decreasing the evaporation rate, the temperature of the collected surface and the pressure of the carrier gas as well as using carrier gases of lower molecular mass. Lighter inert gases lead to smaller particles [22,24].

Granqvist and Buhrman were the pioneers in using this technique for the growth of metal nanoparticles in He, Ar or Xe atmospheres at different pressures [22]. Other researchers have used the IGC method for fabricating Ag [24], Au [25], SnO [26], Mn-oxides [27] and ZrO_{2-x} [28] nanoparticles. In these cases He or Ar were used as a carrier gas, sometimes mixed with oxygen for growing metal oxide particles. There are few works that use H_2 as the carrier gas for the growth of metal nanoparticles by means of the gas condensation method [30]. Hydrogen is lighter than helium and has more degrees of freedom; therefore, it has a lower confinement capacity and a higher cooling rate [29], which could lead to the growth of smaller particles using the IGC process. However, Pfau et

* Corresponding author. Present address: Departamento de Física, Facultad de Física, Pontificia Universidad Católica de Chile, Santiago, Chile. Tel.: +56 2 978 4338; fax: +56 2 6967359.
E-mail address: dodiaz@fis.puc.cl (D.E. Diaz-Droguett).

0169-4332/$ – see front matter © 2010 Elsevier B.V. All rights reserved.
doi:10.1016/j.apsusc.2010.12.082

al. grew nanoclusters of Pb and Bi with the IGC method using He carrier gas, but they could not obtain these nanoclusters using H_2 since the particles became too large [30].

The present work reports on the synthesis, structural and morphological characterization of copper nanoparticles. They were grown by means of the IGC method using H_2 instead of an inert gas, at pressures between 10 and 1200 Pa. The aim of this research is twofold. The first goal is determining if nano-sized copper particles can be grown under H_2 at the defined pressure range and the second one is to study the surface oxide characteristics of these nanoparticles.

2. Experimental procedure

2.1. Preparation of copper nanoparticles in hydrogen

The preparation consisted in evaporating 1 g of copper (OFHC: oxygen free high conductivity) from a resistive source (tungsten boat) under H_2 (AGA, 99.995%, O_2 <5 ppm and H_2O <4 ppm) atmospheres at pressures from 10 to 1200 Pa. The procedure and the experimental setup for the growth of nanoparticles using this technique have already been described elsewhere [23,31].

The tungsten boat is placed inside a high vacuum chamber that was evacuated up to a pressure around 10^{-4} Pa. A mass spectrometer was used to monitor the partial pressure of the active gases, mainly oxygen (10^{-6} Pa), nitrogen (10^{-6} Pa) and water vapor (10^{-5} Pa). Then hydrogen was injected to reach the operating pressure (10–1200 Pa). The pressure was measured with absolute (capacitive) pressure gauges.

The tungsten boat was resistively heated until the working temperature was achieved. The temperatures used ranged from 1320 °C to 1500 °C and were measured with an optical pyrometer through a sapphire window. The material was collected on the surface of a copper semi cylinder cooled with liquid nitrogen and located 75 mm above the tungsten boat. After the evaporation was finished, the high vacuum chamber was left overnight to allow it to reach room temperature and ventilated with air before opening it to remove the nanoparticles from the surface of the collector.

2.2. Characterization

The surface chemical information of the samples was obtained from X-ray photoelectron spectroscopy (XPS, Physical Electronics system model 1257), using either Al or Mg Kα emission. Binding energy and oxidation states were obtained from high resolution scans. The energy scale was calibrated by assigning 284.8 eV to the C 1s adventitious peak. Structural information of the samples was obtained by X-ray diffraction in 2–80° scans (Siemens D5000 powder diffractometer) using a graphite monochromator and Cu Kα radiation, λ = 0.15406 nm. The morphology of the samples was examined using a TEM/HRTEM JEOL 2010 microscope operating at 200 kV and under diffraction and phase contrast modes. This instrument is also equipped with selected area electron diffraction (SAED) for the crystallographic information of the samples.

3. Results

3.1. Preparation conditions, yields and crystals size

The preparation conditions determined by the partial pressure of hydrogen and the maximum temperature of the evaporation source, as well as the yield of each evaporation, are listed in Table 1. The amounts obtained in all the evaporations were below 0.45 g on each occasion, with variable yields that did not exceed 42%.

Table 1
Preparation conditions and evaporation yield of copper under hydrogen atmosphere.

Condition	Partial pressure (Pa)	Sourer temperature (°C)	Yield* (%)	Crystalline size (1 1 1) (nm)
1	10	1726 ± 4	13	25
2	50	1494 ± 5	13	11
3	100	1420 ± 5	11	21
4	200	1350 ± 6	37	15
5	400	1499 ± 5	25	18
6	600	1322 ± 8	11	10
7	800	1337 ± 7	12	14
8	1000	1429 ± 5	26	15
9	1200	1427 ± 5	42	16

* The yields were calculated as the mass percentage of the powder deposited on the collecting substrate with respect to the Cu mass used in the evaporation.

3.2. Characterization of the samples: structural and morphological

3.2.1. X-ray diffraction (XRD)

Fig. 1 shows X-ray diffraction patterns of copper nanoparticles grown under different preparation conditions. The XRD results revealed the reflections of metallic copper sometimes mixed with an oxidized phase (Cu_xO, $x = 1, 2$). Diffractgrams (a), (b), (c), (f) and (g), corresponding to the samples grown under conditions 1, 2, 3, 6 and 7, respectively, exhibit the reflections of the Cu cubic

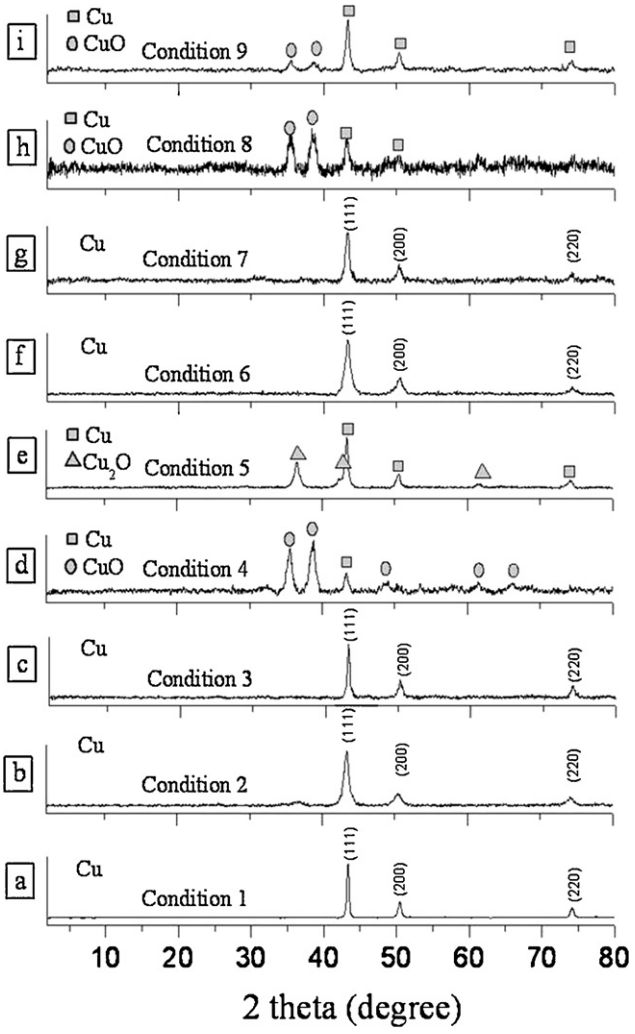

Fig. 1. XRD patterns of nanoparticles grown under different preparation conditions.

crystal structure with lattice constant $a = 0.3615$ nm, in agreement with the standard published data (PDF card no. 04-0836). Diffractograms (d), (h) and (i), which correspond to the samples grown under conditions 4, 8 and 9, respectively, displayed reflections that can be indexed to Cu cubic structure (PDF card no. 04-0836) and to CuO monoclinic crystal structure. The oxide lattice constants are $a = 0.4683$ nm, $b = 0.3421$ nm, $c = 0.5129$ nm, and $\beta = 99.567^\circ$, in agreement with the published data (PDF card no. 80-1266). Pattern (e) from the sample grown under condition 5 was the only one revealing the presence of cuprous oxide. These reflections came from Cu crystal structure (PDF card no. 04-0836) and Cu_2O cubic crystal structure with lattice constant $a = 0.4258$ nm, in agreement with the standard data (PDF card no. 77-0199). In some cases, the diffractograms had broader and less defined reflections due to the different average sizes of the nanoparticles.

3.2.2. Crystallite size by XRD

The determination of the crystallite size (L_c) of the copper nanoparticles was performed using Scherrer's equation [32]:

$$L_c = \frac{k\lambda}{\beta \cos\theta} \quad (1)$$

where k is the shape coefficient (between 0.9 and 1.0), λ is the X-ray wave length, β is the full width at half maximum (FWHM) of each peak and θ is the diffraction angle. For this purpose, we chose the peak of the (1 1 1) plane near 43.32° in the pattern of the copper nanoparticles. A silicon wafer was used pattern to determine the instrumental width ($w_{inst} = 0.022$) and then to calculate the crystallite size using Eq. (1).

The β parameter must be corrected using the following equation [33]:

$$\beta = \sqrt{w_{exp}^2 - w_{inst}^2} \quad (2)$$

where w_{exp} is the experimental FWHM obtained for each sample. The crystal sizes for all samples, assuming $k = 0.9$, are presented in Table 1. From these values it is not possible to establish a correlation between the partial pressure of hydrogen and the preparation conditions with the crystallite size measured by XRD. Nevertheless, the XRD patterns indicate that the grain size for the samples prepared under different conditions is within the range of 10–25 nm.

3.2.3. Transmission electron microscopy (TEM)

Fig. 2 shows a cumulus of agglomerated nanoparticles prepared under a partial pressure of hydrogen of 400 Pa (condition 5). The couple of bright field (BF) and dark field (DF) images allow a particle diameter estimation of 12 nm for this condition. The inset image shows the diffraction pattern (DP) of the cumulus of particles in which the diffraction rings identify the copper structure.

Fig. 3 shows dispersed rounded copper nanoparticles prepared in hydrogen under a pressure of 200 Pa (condition 4). Fig. 3(a) shows an average diameter of 9.1 ± 0.3 nm, while Fig. 3(b) displays faceted particles not exceeding 25 nm.

Most of the copper nanoparticles grown at the different conditions under hydrogen were single crystals with some of them containing a twin boundary. Fig. 4 shows a BF image of particles prepared under condition 4. The inset is a DP taken from the framed particle revealing its single crystal character with well-defined diffraction spots. Particles about 10 nm indicated by the arrows also can be detected in Fig. 4

Fig. 5 shows a couple of BF/DF images of a twinned particle of 80 nm in diameter grown under condition 4. Particles containing twin boundaries appeared often under the different preparation conditions. The generation of twins is a typical defect in copper, formed during the coalescence process of the copper clusters [14,34].

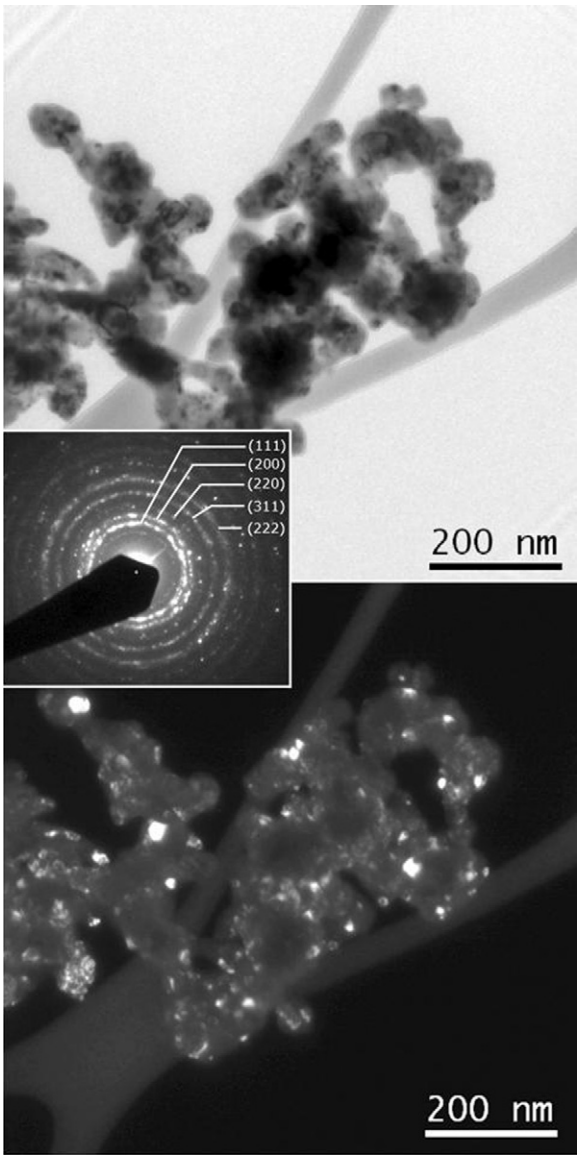

Fig. 2. Bright and dark field images of copper nanoparticles prepared under 400 Pa of hydrogen partial pressure (condition 5).

In general, the TEM examination of the samples grown under the different conditions determined that the size of the nanoparticles is within the 10–50 nm range, which is in agreement with the crystallite values obtained by XRD.

3.3. Characterization of the surface oxide by X-ray photoelectron spectroscopy (XPS)

3.3.1. Characterization of as-received samples

XPS spectra revealed that the samples grown under the different conditions only contain copper and oxygen, and allowed the identification of the surface oxide on the nanoparticles. Fig. 6 depicts XPS spectra revealing the chemical composition and the oxidation state of an as-prepared sample grown under condition 4 (200 Pa, 1350 °C). The survey spectrum shows the copper photoelectron peaks (Cu3s, $Cu2p_{1/2}$, $Cu2p_{3/2}$, Cu3p and its CuLMM Auger), the oxygen peaks (O1s and its OKLL Auger) and the photoelectron peak of the adventitious carbon (C1s). No impurities on the surface of the particles were detected. The inset of Fig. 6 is the narrow range of the Cu2p spectral zone (framed rectangle) showing the character-

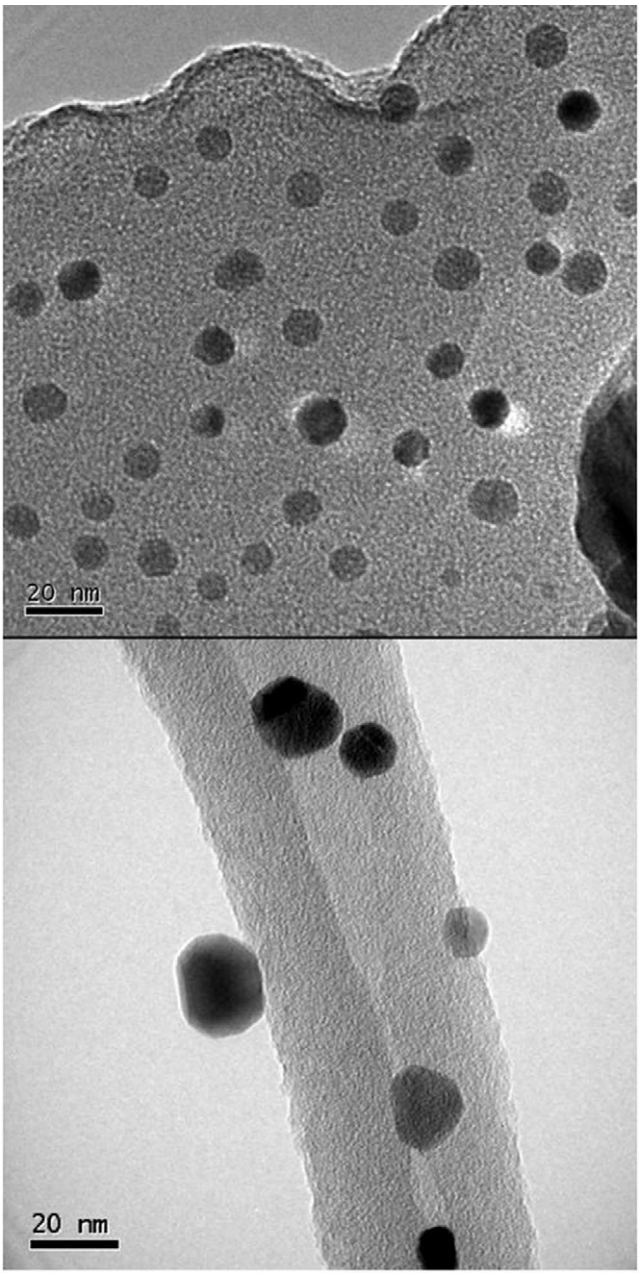

Fig. 3. Copper nanoparticles prepared under 200 Pa of hydrogen partial pressure (condition 4).

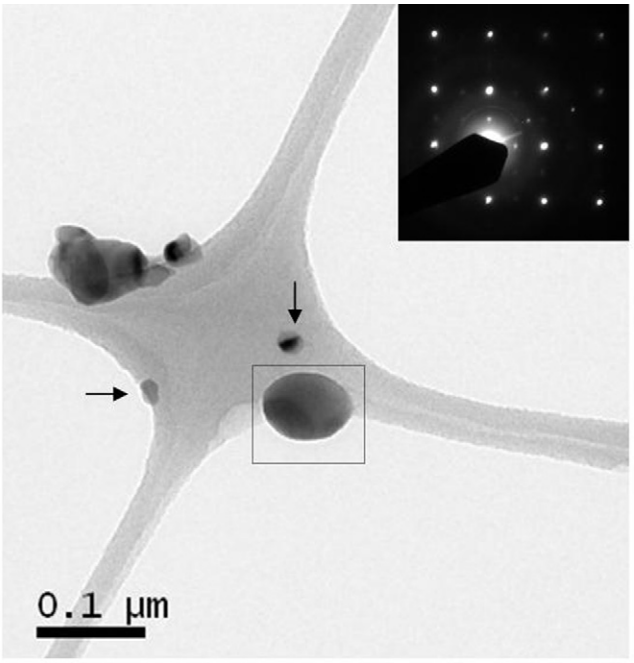

Fig. 4. Copper nanoparticles prepared under 200 Pa of hydrogen partial pressure (condition 4). The Inset is a DP pattern of the framed particle.

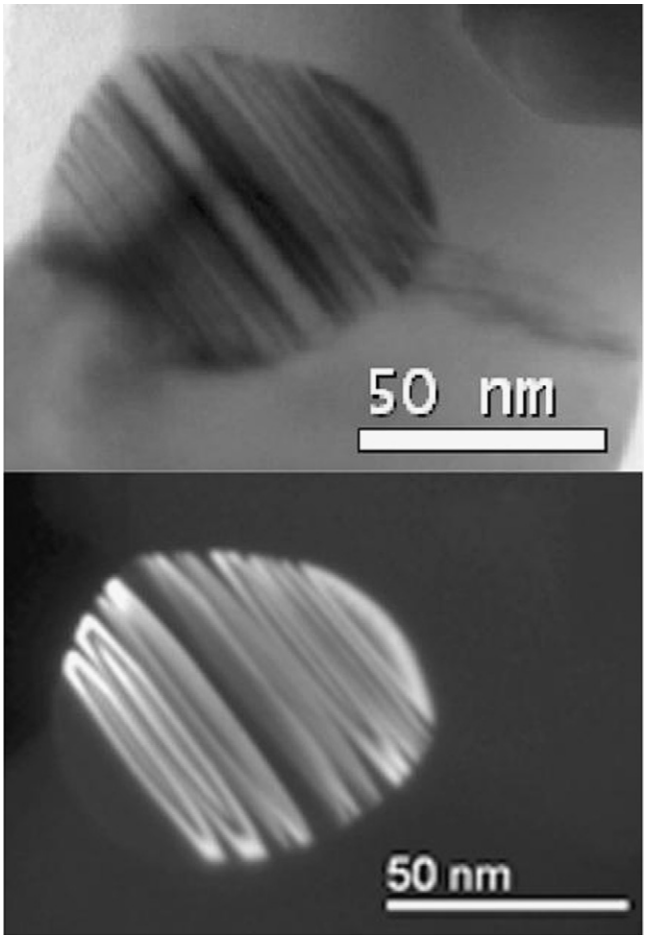

Fig. 5. BF/DF image of a twinned particle prepared under 200 Pa of hydrogen partial pressure (under condition 4).

istic shake-up satellites of CuO (s_1: $2p_{1/2}3d^9$ and s_2: $2p_{3/2}3d^9$). This analysis corroborates the XRD result of this sample which displayed some reflections of the CuO phase along with a weak reflection of Cu(1 1 1), as shown in diffractogram (d) of Fig. 1. The formation of oxide on the copper nanoparticles surface is due to the air exposure when the samples are removed from the collecting substrate of the preparation chamber.

3.3.2. Ar^+-sputtered samples

Studies on the $CuL_3M_{45}M_{45}$ Auger peaks and the $Cu2p_{3/2}$ photoelectron peaks from the samples revealed that the composition of the oxide from the surface of the nanoparticles consisted of a CuO layer over one of Cu_2O. The $CuL_3M_{45}M_{45}$ Auger peak in the XPS spectra was studied to distinguish between Cu and Cu_2O, since they cannot be resolved only by measuring the binding energy of the $Cu2p_{3/2}$ peak, because their binding energies are too close (they

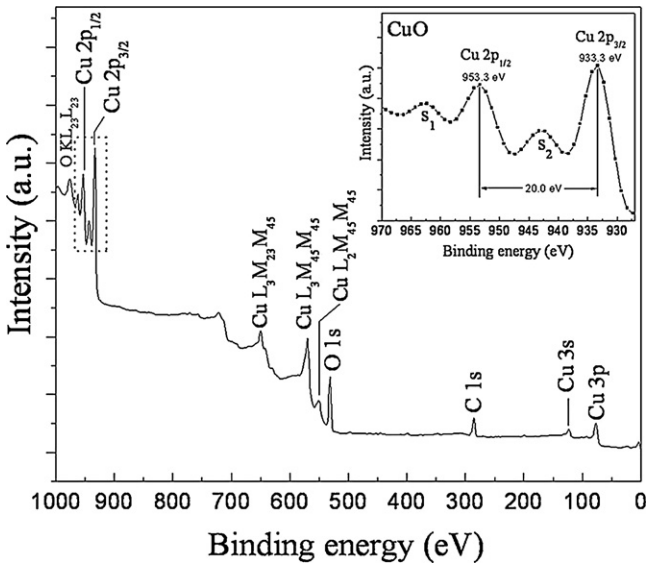

Fig. 6. XPS spectra of an as-prepared sample grown under condition 4 (200 Pa, 1350 °C).

differ by only 0.1 eV), whereas the position of the Auger peak for Cu and Cu_2O are located at 568.0 eV and 570.0 eV, respectively [35].

Fig. 7 shows high resolution spectra of the same sample of Fig. 6 made using condition 4 (200 Pa, 1350 °C). These spectra were recorded after eroding the copper nanoparticles surface with Ar^+ for 4 min at 1 μA with a beam voltage of 2 kV.

The $CuL_3M_{45}M_{45}$ Auger peak is located at 569.9 eV, close to reported value of 570.0 eV for Cu_2O [35]. The Auger parameter (A.P.) plus the photon energy was 1849.3 eV, which corresponds to Cu_2O [36] and corroborates our previous result.

The inset of Fig. 7 shows that the best fit of the $Cu2p_{3/2}$ photoelectron peak was obtained resolving it into two peaks. The binding energy (BE) of the highest intensity was observed at 932.6 eV (FWHM ~1.8) corresponding to copper in Cu_2O, whereas the BE of the lower intensity observed at 934.3 eV (FWHM ~2.2) corresponded to copper in CuO. This last BE value is higher than the reported values of the CuO, which are between 933.6 eV and 933.9 eV [37–42]. It has been reported that when the content of surface CuO is low, the BE shifts to a higher value of 934.4 eV [37,43] which is close to the value measured here (934.3 eV). On the other hand, the BE of Cu(I), which was the dominant signal after Ar^+-sputtering, was slightly higher than the reported values of 932.4 eV or 932.5 eV [44].

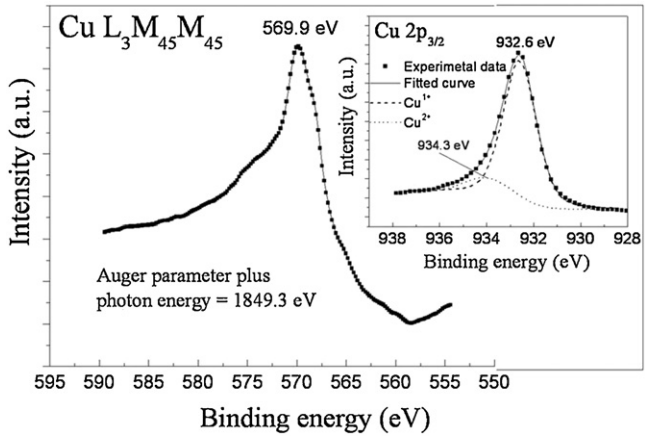

Fig. 7. High resolution spectra from the same sample studied in Fig. 6 (condition 4). $CuL_3M_{45}M_{45}$ Auger signal and fitting of its $Cu2p_{3/2}$ peak (inset). These spectra were recorded after Ar^+-erosion.

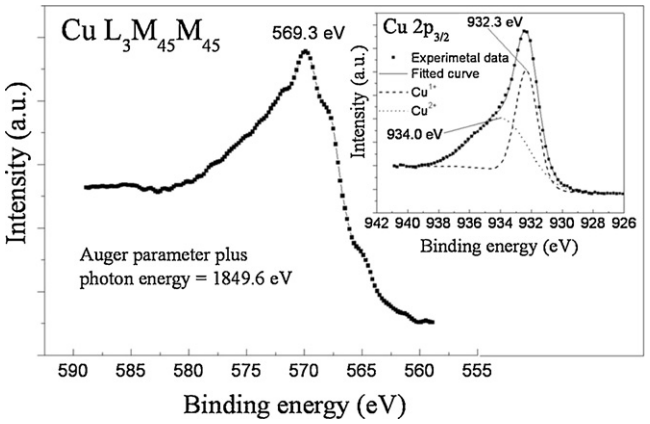

Fig. 8. High resolution spectra of a sample grown under condition 2 (50 Pa, 1494 °C). The CuL3M45M45 Auger signal and fitting of its Cu2p3/2 peak (inset). These spectra were recorded after Ar^+ erosion.

In conclusion, the XPS analysis (Figs. 6 and 7) revealed the presence of Cu(I) below a thin Cu(II) shell on the copper nanoparticles.

Fig. 8 shows the high resolution XPS spectra of a sample grown under condition 2 (50 Pa, 1494 °C). These spectra were also recorded after eroding the exposed surface of the nanoparticles with Ar^+ under the same conditions (4 min at 1 μA with a beam voltage of 2 kV).

The $CuL_3M_{45}M_{45}$ Auger peak located at 569.3 eV is close to the reported value for Cu_2O (570.0 eV) [35]. The A.P. plus photon energy was of 1849.6 eV, also corresponding to Cu_2O [36], as in the previous case (Fig. 7).

The inset of Fig. 8 shows that the $Cu2p_{3/2}$ photoelectron peak is broader and more asymmetric than the $Cu2p_{3/2}$ peak analyzed previously (Fig. 7). This peak also can be fitted with two curves by assigning 932.3 eV to Cu(I) and 934.0 to Cu(II), with a FWHM of 1.8 and 4.4 eV, respectively. The FWHM of the Cu(II) peak is broader and more distorted than the one for Cu(I). This may be used indirectly to indicate that the photoelectrons responsible of the Cu(II) peak come from a very thin CuO layer that is coating the Cu_2O shell [45]. The BE of Cu(I) is slightly lower than the reported values for Cu_2O at 932.4 eV or 932.5 eV [44].

The layer of CuO and Cu_2O on the nanoparticles is very thin. Therefore, the low oxide content in this sample (as inferred from XPS) is consistent with its XRD analyses that did not detect oxidized phases and only exhibited the copper reflections, as shown in Fig. 1b).

4. Discussion

4.1. Stable oxide in copper nanoparticles

The standard formation enthalpy of CuO and Cu_2O are −168,6 kJ/mol and −157,3 kJ/mol, respectively, and the corresponding Gibbs energies are −146 kJ/mol and −129,7 kJ/mol [46]. In an oxidizing atmosphere such as air, Cu_2O oxidizes to CuO. These thermodynamic considerations hold for macroscopic samples. Our own XPS studies on copper nanoparticles with sizes from 10 nm to 50 nm revealed a CuO layer over a Cu_2O shell that covers the copper core, with Cu(I) being the main oxidation state after Ar^+ erosion (as shown by the Auger peaks and fitting of the $Cu2p_{3/2}$ spectra), suggesting that Cu_2O is the most stable phase on the nanoparticles or that the oxidation kinetics to CuO is particularly slow.

Our observation is in line with reports of Teo [43] and Balamurugan [47] that report that a small fraction of surface Cu_2O is oxidized

to CuO during sample drying and handling under normal ambient conditions. The phase of Cu_2O in nanoparticles of different sizes has been the subject of several studies. Balamurugan et al. showed that at smaller particle size the more symmetric cubic Cu_2O phase should be more stable than the monoclinic CuO phase [47]. Palkar et al. studied the effect of reducing sizes on the stability of Cu_2O and CuO [48]. They postulated that smaller particle sizes should enhance the ionic character of the Cu–O system and the tendency towards structures of comparatively higher symmetry (CuO is a covalent oxide with a low symmetry structure whereas Cu_2O has a high-symmetry structure and a lower anion/cation ratio, which is more stable at a small particle size). Huang et al. prepared Cu_2O particles using liquid phase chemical synthesis and found that Cu(I) was the main oxidation state present on the surface of the smaller particles (~90 nm), whereas Cu(II) was the main state on the surface of the microparticles (~1.5 μm) [49]. Ghodselahi et al. reported on XPS measurements of copper nanoparticles grown using sputtering on a supporting substrate. Despite the different preparation conditions, they had the same observation: after exposure to air, the shell of the nanoparticles was mainly Cu_2O coated with a thin CuO layer [45]. Salavati-Niasari and Davar also showed that a Cu_2O shell was formed when copper nanoparticles (~10 nm) synthesized by thermal decomposition of $[Cu(sal)_2]$-oleylamine complex were exposed to air [18]. These observations indicate that the Cu_2O shell with at a thin CuO layer is a size dependent property of the nanoparticles and not a consequence of a particular preparation method.

5. Conclusions

Copper nanoparticles of diameters between 10 and 50 nm were grown using the gas condensation method with hydrogen at pressures from 10 to 1200 Pa as carrier gas. The TEM examination showed single crystal particles with well-faceted shapes sometimes containing twin boundaries. No correlation between the gas pressure and the crystallite size was found. XPS analyses revealed that the copper nanoparticles were covered by a Cu_2O shell surrounding the copper core and a with a CuO external layer. The stable oxide and the main oxidation state around the nanoparticles was Cu_2O with only a thin surface layer of CuO. It seems that this behavior does not depend on the preparation method and is a property of the nanoparticles.

Acknowledgments

This work has been partially funded by the Chilean government under contract FONDECYT 1070789 and MECESUP UCH0205. We acknowledge the discussions with Dr. M.E. Pilleux. D.E. Díaz-Droguett acknowledges a CONICYT fellowship.

References

[1] G. Vitulli, M. Bernini, S. Bertozzi, E. Pitzalis, P. Salvadori, S. Coluccia, G. Martra, Chem. Mater. 14 (2002) 1183.
[2] H.H. Huang, F.Q. Yan, Y.M. Kek, C.H. Chew, G.Q. Xu, W. Ji, P.S. Oh, S.H. Tang, Langmuir 13 (1997) 172.
[3] A. Bose, S. Basu, S. Banerjee, D. Chakravorty, J. Appl. Phys. 98 (2005), 074307.
[4] N. Cioffi, N. Ditaranto, L. Torsi, R.A. Picca, L. Sabbatini, A. Valentini, L. Novello, G. Tantillo, T. Bleve-Zacheo, P.G. Zambonin, Anal. Bioanal. Chem. 381 (2005) 607–616.
[5] G. Ren, D. Hu, E.W.C. Cheng, M.A. Vargas-Reus, P. Reip, R.P. Allaker, Int. J. Antimicrob. Agents 33 (2009) 587–590.
[6] H. Palza, S. Gutiérrez, K. Delgado, O. Salazar, V. Fuenzalida, J. Avila, G. Figueroa, R. Quijada, Macromol. Rapid Commun. 31 (2010) 563–567.
[7] G. Liu, X. Li, B. Qin, D. Xing, Y. Guo, R. Fan, Tribol. Lett. 17 (4) (2004) 961–966.
[8] Y. Lee, J. Choi, K.J. Lee, N.E. Stott, D. Kim, Nanotechnology 19 (2008) 1–7.
[9] J.G. Lu, P. Chang, Z. Fan, Mater. Sci. Eng., R 52 (2006) 49.
[10] Y. Qu, X. Li, G. Chen, H. Zhang, Y. Chen, Mater. Lett. 62 (2008) 886.
[11] S. Anandan, X.G. Wen, S.H. Yang, Mater. Chem. Phys. 93 (2005) 35.
[12] P.E. de Jongh, D. Vanmaekelbergh, J.J. Kelly, J. Electrochem. Soc. 147 (2) (2000) 486.
[13] I. Aruna, F.E. Kruis, Eur. Aerosol Conf. Salzburg, 2007.
[14] B.K. Park, S. Jeong, D. Kim, J. Moon, S. Lim, J.S. Kim, J. Colloid Interface Sci. 311 (2007) 417–424.
[15] T. Xin-ling, R. Ling, S. Ling-na, I. Wei-guo, C. Min-hua, H. Chang-wen, Chem. Res. Chin. Univ. 22 (2006) 547–551.
[16] P.K. Khanna, S. Gaikwad, P.V. Adhyapak, N. Singh, R. Marimuthu, Mater. Lett. 61 (2007) 4711–4714.
[17] L. Yu, H. Sun, J. He, D. Wang, X. Jin, X. Hu, G.Z. Chen, Electrochem. Commun. 9 (2007) 1374–1381.
[18] M. Salavati-Niasari, F. Davar, Mater. Lett. 63 (2009) 441–443.
[19] M. Saito, K. Yasukawa, T. Umeda, Y. Aoi, Opt. Mater. 30 (2008) 1201–1204.
[20] F. Zhou, R. Zhou, X. Hao, X. Wu, W. Rao, Y. Chen, D. Gao, Radiat. Phys. Chem. 77 (2008) 169–173.
[21] H. Zhu, C. Zhang, Y. Yin, Nanotechnology 16 (2005) 3079–3084.
[22] C.G. Granqvist, R.A. Buhrman, J. Appl. Phys. 47 (1976) 2200.
[23] D.E. Díaz-Droguett, V.M. Fuenzalida, J. Nanosci. Nanotechnol. 10 (2010) 6694–6706.
[24] M. Turker, Mater. Sci. Eng. A (2004) 36774–36781.
[25] K.-M. Lee, S.-T. Park, D.-J. Lee, J. Alloys Compd. (2004).
[26] K.-M. Lee, D.-J. Lee, H. Ahn, Mater. Lett. 58 (2004) 3122–3125.
[27] L. Dimesso, L. Heider, H. Hahn, Solid State Ionics 123 (1999) 39–46.
[28] M. Nagashima, T. Nakayama, S. Yamanaka, M. Fujikane, Y. Hayashi, T. Sekino, T. Kusunose, K. Niihara, Mater. Lett. 57 (2003) 4023–4027.
[29] P. Heszler, L. Landström, C.G. Granqvist, Basics of UV laser-assisted generation of nanoparticles, in: C. Granqvist, L. Kisch, W. Marlow (Eds.), Gas Phase Nanoparticles Synthesis, Kluwer Academic Publishers, Dordrecht, Boston, London, 2004, p. 82.
[30] P. Pfau, K. Sattler, J. Mühlbach, R. Pflaum, E. Recknagel, J. Phys. F: Met. Phys. 12 (1982) 2131–2139.
[31] D.E. Díaz-Droguett, V.M. Fuenzalida, G. Solórzano, J. Nanosci. Nanotechnol. 8 (2008) 5977.
[32] B.D. Cullity, S.R. Stock, Elements of X-Ray Diffraction, 3rd ed., Prentice-Hall, Inc., New Jersey, 2001.
[33] A.F.L. Almeida, R.S. de Oliveira, J.C. Góes, J.M. Sasaki, A.G. Souza Filho, J. Mendes Filho, A.S.B. Sombra, Mater. Sci. Eng., B 96 (3) (2002) 275–283.
[34] C. Duhamel, J.L. Bonnentien, Y. Champion, J. Alloys Compd. 460 (1–2) (2008) 191–195.
[35] J.-Y. Park, J. Yeon-sik jung, W.-K. Cho, Choi, Appl. Surf. Sci. 252 (2006) 5877.
[36] J.F. Moulder, W.F. Stickle, P.E. Sobol, K.D. Bomben, Handbook of X-Ray Photoelectron Spectroscopy Physical Electronics Division, Perkin-Elmer, Eden Prairie, Minnesota, 1992.
[37] J.P. Espinos, J. Morales, A. Barranco, A. Caballero, J.P. Holgado, A.R. Gonzalez-Elipe, J. Phys. Chem. B 106 (2002) 6921.
[38] W. Wang, Z. Liu, Y. Liu, C. Xu, C. Zheng, G. Wang, Appl. Phys. A 76 (2003) 417.
[39] J.W. Zhu, H.Q. Chen, H.B. Liu, X.J. Yang, L.D. Lu, W. Xin, Mater. Sci. Eng., A 384 (2004) 172.
[40] M.A. Brookshier, C.C. Chusuei, D.W. Goodman, Langmuir 15 (1999) 2043.
[41] W.Z. Wang, Y.J. Zhan, X.S. Wang, Y.K. Liu, C.L. Zheng, G.H. Wang, Mater. Res. Bull. 37 (2002) 1093.
[42] H. Wang, J.Z. Xu, J.J. Zhu, H.Y. Chen, J. Cryst. Growth 244 (2002) 88.
[43] J.J. Teo, Y. Chang, H.C. Zeng, Langmuir 22 (2006) 7369.
[44] W.Z. Wang, G.H. Wang, S.X. Wang, Y.J. Zhan, Y.K. Liu, C.L. Zheng, Adv. Mater. 14 (2002) 67.
[45] T. Ghodselahi, M.A. Vesaghi, A. Shafiekhani, A. Baghizadeh, M. Lameii, Appl. Surf. Sci. 255 (2008) 2730–2734.
[46] R.C. Weast, D.R. Lide (Eds.), CRC Handbook Of Chemistry and Physics: A Ready Reference Book of Chemical and Physical Data, 70th ed., CRC Press, Boca Raton, 1989.
[47] B. Balamurugan, B.R. Mehta, S.M. Shivaprasad, Appl. Phys. Lett. 79 (2001) 3176.
[48] V.R. Palkar, P. Ayyub, S. Chattopadhyay, M. Multani, Phys. Rev. B 53 (1996) 2167.
[49] L. Huang, F. Peng, H. Yu, H. Wang, Solid State Sci. 11 (2009) 129–138.